J|A|C|S
ARTICLES
Published on Web 04/10/2007

4-Aryl-1,3,2-oxathiazolylium-5-olates as pH-Controlled NO-Donors: The Next Generation of *S*-Nitrosothiols

Dongning Lu,[†] Janos Nadas,[†] Guisheng Zhang,[§] Wesley Johnson,[‡] Jay L. Zweier,[‡] Arturo J. Cardounel,[‡] Frederick A. Villamena,*[,‡] and Peng George Wang*[,†]

Contribution from the Departments of Biochemistry and Chemistry, and The Davis Heart and Lung Research Institute, and Division of Cardiovascular Medicine, Department of Internal Medicine, College of Medicine, The Ohio State University, Columbus, Ohio 43210, and College of Chemistry and Environmental Science, Henan Normal University, Henan Xinxiang 453007, People's Republic of China

Received November 16, 2006; E-mail: wang.892@osu.edu; frederick.villamena@osumc.edu

Abstract: *S*-Nitrosothiols (RSNOs) are important exogenous and endogenous sources of nitric oxide (NO) in biological systems. A series of 4-aryl-1,3,2-oxathiazolylium-5-olates derivatives with varying aryl para-substituents ($-CF_3$, $-H$, $-Cl$, and $-OCH_3$) were synthesized. These compounds were found to release NO under acidic condition (pH = 5). The decomposition pathway of the aryloxathiazolyliumolates proceeded via an acid-catalyzed ring-opening mechanism after which NO was released and an S-centered radical was generated. Electron paramagnetic resonance (EPR) spin trapping studies were performed to detect NO and the S-centered radical using the spin traps of iron(II) *N*-methyl-D-glucamine dithiocarbamate [$(MGD)_2-Fe^{II}$] and 5,5-dimethyl-1-pyrroline *N*-oxide (DMPO). Also, EPR spin trapping and UV−vis spectrophotometry were used to analyze the effect of aryl para substitution on the NO-releasing property of aryloxathiazolyliumolates. The results showed that the presence of an electron-withdrawing substituent such as $-CF_3$ enhanced the NO-releasing capability of the aryloxathiazolyliumolates, whereas an electron-donating substituent like methoxy ($-OCH_3$) diminished it. Computational studies using density functional theory (DFT) at the PCM/B3LYP/6-31+G**//B3LYP/6-31G* level were used to rationalize the experimental observations. The aryloxathiazolyliumolates diminished susceptibility to reduction by ascorbate or gluthathione, and their capacity to cause vasodilation as compared to other *S*-nitrosothiols suggests potential application in biological systems.

Introduction

One of the biggest discoveries in the past decade was the identification of nitric oxide (NO) as a signaling molecule in cells and tissues.[1] Since then, NO has been shown to participate in a variety of biological functions,[2,3] including the normal physiological control of vessel dilatation, neurotransmission, macrophage-induced cytostatics, and cytotoxicity.[4]

S-Nitrosothiol (RSNOs) species are NO-donor compounds that are wildly distributed in vivo and have been shown to store, transport, and release nitric oxide within the mammalian body. For example, in the blood, *S*-nitrosoalbumin (SNO-albumin) and *S*-nitrosohemoglobin (SNO-Hb) have been reported to constitute the major conduits for circulating NO bioactivity,[5] and the low-molecular-weight RSNOs, such as *S*-nitrosoglutathione (GSNO) (Figure 1) and *S*-nitrosocysteine (CysNO), have been proposed as mediators of paracrine protein S-nitrosylation.[6] Furthermore, S-nitrosylation can regulate protein function, as has been described for numerous proteins.[7−11] Therefore, the creation of synthetic donors, mimicking the endogenous low-molecular-weight RSNOs for research and therapeutic applications, has become extremely enticing.[12−20]

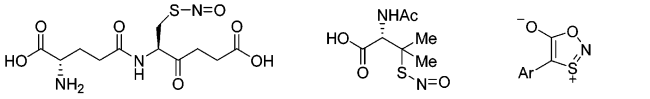

Figure 1. Structures of *S*-nitrosoglutathione (GSNO), *S*-nitroso-*N*-acetylpenicillamine (SNAP), and aryloxathiazolyliumolates.

[†] Departments of Biochemistry and Chemistry, The Ohio State University.
[‡] The Davis Heart and Lung Research Institute, and Department of Internal Medicine, The Ohio State University.
[§] Henan Normal University.

(1) Ignarro, L. J. *Nitric Oxide* **1996**, 111.
(2) Ignarro, L. J., Murad, F., Eds. Nitric Oxide: Biochemistry, Molecular Biology, and Therapeutic Implications. *Adv. Pharmacol.* **1995**, *34*, 530.
(3) Lancaster, J., Jr., Ed. *Nitric Oxide: Principles and Actions*; 1996; p 355.
(4) Ignarro, L. J., Ed. *Nitric Oxide: Biology and Pathobiology*; 2000; p 1003.
(5) Foster, M. W.; Pawloski, J. R.; Singel, D. J.; Stamler, J. S. *Hypertension* **2004**, *45*, 15.
(6) Zhang, Y.; Hogg, N. *Am. J. Physiol.* **2004**, *287*, L467.
(7) Lipton, S. A.; Choi, Y. B.; Pan, Z. H.; Lei, S. Z.; Chen, H. S.; Sucher, N. J.; Loscalzo, J.; Singel, D. J.; Stamler, J. S. *Nature* **1993**, *364*, 626.
(8) Lander, H. M.; Ogiste, J. S.; Pearce, S. F.; Levi, R.; Novogrodsky, A. *J. Biol. Chem.* **1995**, *270*, 7017.
(9) Caselli, A.; Camici, G.; Manao, G.; Moneti, G.; Pazzagli, L.; Cappugi, G.; Ramponi, G. *J. Biol. Chem.* **1994**, *269*, 24878.
(10) Gopalakrishna, R.; Chen, Z. H.; Gundimeda, U. *J. Biol. Chem.* **1993**, *268*, 27180.
(11) Mohr, S.; Stamler, J. S.; Brune, B. *J. Biol. Chem.* **1996**, *271*, 4209.
(12) Boschi, D.; Tron, G. C.; Di Stilo, A.; Fruttero, R.; Gasco, A.; Poggesi, E.; Motta, G.; Leonardi, A. *J. Med. Chem.* **2003**, *46*, 3762.
(13) Cai, T. B.; Lu, D.; Landerholm, M.; Wang, P. G. *Org. Lett.* **2004**, *6*, 4203.
(14) Cai, T. B.; Lu, D.; Tang, X.; Zhang, Y.; Landerholm, M.; Wang, P. G. *J. Org. Chem.* **2005**, *70*, 3518.
(15) Huang, J.; Kim-Shapiro, D. B.; King, S. B. *J. Med. Chem.* **2004**, *47*, 3495.

The most commonly used synthetic RSNO is *S*-nitroso-*N*-acetylpenicillamine (SNAP) (Figure 1), which can induce apoptosis in a neuronal cell line by the production of different reactive molecules.[21] Other RSNOs have been found to inactivate aconitase and inhibit the uptake of norepinephrine in sympathetic neurons.[22,23] In addition, RSNOs may directly serve as drug in the treatment of a variety of diseases such as hypertension,[24] atherosclerosis,[25] and congestive heart failure.[26] RSNOs can also be used as potent antiplatelet agent and vasodilator. Even though most of these biological functions are usually attributed to NO release, it has been suggested that RSNOs can also exhibit direct effects without NO generation such as S-nitrosation of protein systems.[27] An additional important function of RSNOs is in stress response during GSH depletion, which may contribute to the well-known oxidant signaling pathways.[28,29] Therefore, the design and synthesis of novel *S*-nitrosothiols exhibiting better pharmacokinetic properties have been the focus in this field for a long time.[30]

A series of novel sugar-*S*-nitrosothiols (sugar-SNAPs), developed by Wang and co-workers,[31] have shown better water solubility, cell penetration, and drug−receptor interaction. Butler and co-workers[32] have also developed a series of novel *S*-nitroso-1-thiolsugars, which have both hydrophobic and hydrophilic groups, allowing them to be delivered transdermally. A number of *S*-nitroso peptides[33] have also been synthesized with considerable stability in the presence of copper ion as compared to SNAP.

Despite the enormous biomedical potential of *S*-nitrosothiols, they are unstable in solution due to the S−N bond being weak, sterically hindered, or strongly polarized. The general instability of the S−N bond leads to low S−NO homolytic/heterolytic bond dissociation energies.[34] The estimated homolytic bond dissociation energy is between 22 and 32 kcal/mol.[35,36] Also, the stability of *S*-nitrosothiols appears to be influenced by the structure of the organic substituent with the primary and secondary RSNOs reported to be highly unstable with half-lives of seconds to minutes,[37] whereas tertiary RSNOs such as those derived from SNAP have been isolated and are indefinitely stable due to the bulkiness of the alkyl group.[38]

Scheme 1. Photo- and Thermal Decomposition of 1,3,2-Oxathiazolium-5-olates

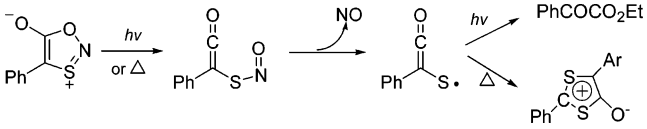

Because the general instability of *S*-nitrosothiols has made them difficult to study, a lot of research has been done in improving their stability. Electronic and steric effects primarily determine their stability. For example, evidence has shown that a small pool of protein *S*-nitrosothiols are stable for hours in the intracellular environment due to either electronic static or steric factors.[39] Yet, exogenously, the most efficient synthetic approaches to making more stable *S*-nitrosothiols have been focused on the tertiary RSNOs derivatives. Thus, the exploration is limited by the chemical structure of the R group, which also makes it more difficult to fine-tune the stability of these compounds.

One novel approach to solve this problem is to look for a more stable pro-drug of *S*-nitrosothiol that can be converted into a normal *S*-nitrosothiol upon activation. A new class of *S*-nitrosothiol pro-drugs are the 4-aryl-1,3,2-oxathiazolium-5-olates. The synthesis and the chemical and photochemical properties of 4-phenyl-1,3,2-oxathia-zolium-5-olates were first reported by Gotthardt et al. more than three decades ago.[40−43] The structure of 4-aryl-1,3,2-oxathiazolium-5-olates is a cyclic version of an α-*S*-nitroso-α-phenyl acetic acid (Figure 1). Because of this unique cyclic structural feature, aryloxathiazolyliumolates may exhibit better stability as compared to the linear *S*-nitrosothiols, and the relative stability of this series of compounds may be fine-tuned by the different para-substitutions on the aryl ring. Although the NO-releasing property of aryloxathiazolyliumolates has not yet been explored, there is indirect evidence to suggest that NO was generated during photochemical or thermal decomposition (Scheme 1).[40,44] The final products $ArCOCO_2Et$ and hetereocyclic dithioliumolate were formed via a resonance-stabilized phenyl(oxomethylene)-thiyl radical.

Herein, the synthesis, stability, theoretical and experimental mechanistic studies of NO release, and potential biological applications as vasodilating agents of four 4-aryl-1,3,2-oxathiazolylium-5-olate derivatives are presented. This is the first report of the acid-catalyzed decomposition of aryloxathiazolyliumolates in aqueous solution and in biological systems that demonstrates the unique NO-releasing property of these compounds.

(16) Huang, J.; Zou, Z.; Kim-Shapiro, D. B.; Ballas, S. K.; King, S. B. *J. Med. Chem.* **2003**, *46*, 3748.
(17) Jia, Q.; Janczuk, A. J.; Cai, T.; Xian, M.; Wen, Z.; Wang, P. G. *Expert Opin. Ther. Pat.* **2002**, *12*, 819.
(18) Lazzarato, L.; Rolando, B.; Lolli, M. L.; Tron, G. C.; Fruttero, R.; Gasco, A.; Deleide, G.; Guenther, H. L. *J. Med. Chem.* **2005**, *48*, 1322.
(19) Sorba, G.; Galli, U.; Cena, C.; Fruttero, R.; Gasco, A.; Morini, G.; Adami, M.; Coruzzi, G.; Brenciaglia, M. I.; Dubini, F. *ChemBioChem* **2003**, *4*, 899.
(20) Xian, M.; Fujiwara, N.; Wen, Z.; Cai, T.; Kazuma, S.; Janczuk, A. J.; Tang, X.; Telyatnikov, V. V.; Zhang, Y.; Chen, X.; Miyamoto, Y.; Taniguchi, N.; Wang, P. G. *Bioorg. Med. Chem.* **2002**, *10*, 3049.
(21) Terwel, D.; Nieland, L. J. M.; Schutte, B.; Reutelingsperger, C. P. M.; Ramaekers, F. C. S.; Steinbusch, H. W. M. *Eur. J. Pharmacol.* **2000**, *400*, 19.
(22) Bouton, C.; Raveau, M.; Drapier, J. C. *J. Biol. Chem.* **1996**, *271*, 2300.
(23) Kaye, D. M.; Wiviott, S. D.; Kobzik, L.; Kelly, R. A.; Smith, T. W. *Am. J. Physiol.* **1997**, *272*, H875.
(24) Luscher, T. F.; Raij, L.; Vanhoutte, P. M. *Hypertension* **1987**, *9*, 157.
(25) Lefer, A. M.; Sedar, A. W. *Pharmacol. Res.* **1991**, *23*, 1.
(26) Drexler, H.; Hayoz, D.; Munzel, T.; Hornig, B.; Just, H.; Brunner, H. R.; Zelis, R. *Am. J. Cardiol.* **1992**, *69*, 1596.
(27) Bizzozero, O. A.; DeJesus, G.; Howard, T. A. *Neurochem. Res.* **2004**, *29*, 1675.
(28) Zhang, Y.; Hogg, N. Biennial Meeting of the Society for Free Radical Research International, 12th, Buenos Aires, Argentina, May 5−9, 2004; p 167.
(29) Mathews, W. R.; Kerr, S. W. *J. Pharmacol. Exp. Ther.* **1993**, *267*, 1529.
(30) Wang, K.; Zhang, W.; Xian, M.; Hou, Y. C.; Chen, X. C.; Cheng, J. P.; Wang, P. G. *Curr. Med. Chem.* **2000**, *7*, 821.
(31) Hou, Y.; Wang, J.; Andreana, P. R.; Caaantauria, G.; Tarasia, S.; Sharp, L.; Braunschweiger, P. G.; Wang, P. G. *Bioorg. Med. Chem. Lett.* **1999**, *9*, 2255.
(32) Butler, A. R.; Field, R. A.; Greig, I. R.; Flitney, F. W.; Bisland, S. K.; Khan, F.; Belch, J. J. F. *Nitric Oxide* **1997**, *1*, 211.
(33) Butler, A. R.; Al-Sa'doni, H. H.; Megson, I. L.; Flitney, F. W. *Nitric Oxide* **1998**, *2*, 193.
(34) Chen, X.; Wen, Z.; Xian, M.; Wang, K.; Ramachandran, N.; Tang, X.; Schlegel, H. B.; Mutus, B.; Wang, P. G. *J. Org. Chem.* **2001**, *66*, 6064.
(35) Bartberger, M. D.; Mannion, J. D.; Powell, S. C.; Stamler, J. S.; Houk, K. N.; Toone, E. J. *J. Am. Chem. Soc.* **2001**, *123*, 8868.
(36) Stamler, J. S.; Toone, E. J. *Curr. Opin. Chem. Biol.* **2002**, *6*, 779.
(37) Roy, B.; du Moulinet d'Hardemare, A.; Fontecave, M. *J. Org. Chem.* **1994**, *59*, 7019.
(38) Carnahan, G. E.; Lenhert, P. G.; Ravichandran, R. *Acta Crystallogr., Sect. B* **1978**, *B34*, 2645.
(39) Zhang, Y.; Hogg, N. *Free Radical Biol. Med.* **2004**, *36*, 947.
(40) Gotthardt, H. *Chem. Ber.* **1972**, *105*, 2008.
(41) Gotthardt, H. *Tetrahedron Lett.* **1971**, *17*, 1277.
(42) Gotthardt, H. *Chem. Ber.* **1972**, *105*, 196.
(43) Gotthardt, H. *Tetrahedron Lett.* **1971**, *17*, 1281.
(44) Gotthardt, H.; Reiter, F.; Kromer, C. *Liebigs Ann. Chem.* **1981**, *6*, 1025.

Scheme 2. Syntheses of **3a**−**3d**[a]

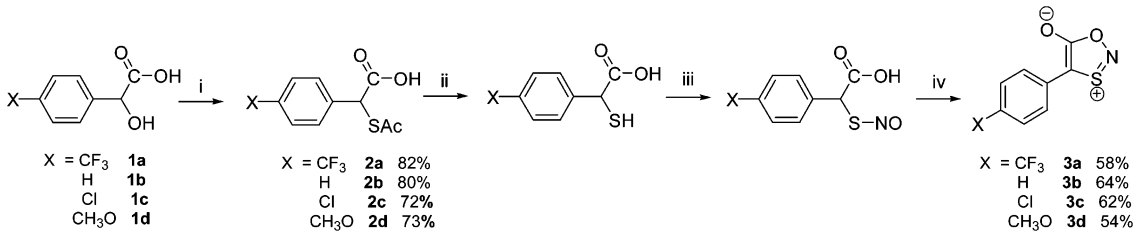

[a] (i) Ph_3P, DIAD, HSAc; (ii) NaOMe/MeOH; (iii) iBuONO/CH_2Cl_2; (iv) DCC/CH_2Cl_2.

Results and Discussion

Synthesis. Four 4-aryl-1,3,2-oxathiazolylium-5-olate compounds (**3a**−**3d**) were synthesized from mandelic acid derivatives **1a**−**1d** (Scheme 2). Compounds **2a**−**2d** are key intermediates for the synthesis of compounds **3a**−**3d**. Literature methods for the syntheses of **2a**−**2d** treated compounds **1a**−**1d** with a mixture of HBr and concentrated H_2SO_4, followed by sodium thioacetate in anhydrous EtOH to afford compounds **2a**−**2d**.[34,44−46] However, this methodology resulted in poor yields and made the product purification very difficult. Moreover, HBr and H_2SO_4 caused the cleavage of the methyl ether in **1d**. In this paper, we opted to exploit the Mitsunobu reaction to prepare the key intermediates **2a**−**2d** because it was a one-step reaction and it provided clean products. The thiol-acetate group was introduced to the α-carbons by treating **1a**−**1d** with triphenyl phosphate, diisopropyl azodicarboxylate (DIAD), and thiolacetic acid to form the compounds **2a**−**2d** with yields of 70−80%. The quantitative deacetylation of **2a**−**2d** was done using sodium methoxide in methanol under inert conditions. The α-aryl-α-mercaptoacetic acid intermediates were nitrosated and then cyclized to afford the heterocyclic compounds **3a**−**3d** in 55−65% yield. Compounds **3a**−**3d** displayed vivid colors depending on the type of substituent on the para-position; that is, electron-withdrawing substituents were yellow solids, while the electron-donating substituents were red. These compounds were soluble in DMSO, acetonitrile, or methylene chloride, but only slightly soluble in water.

Stability Study. In the solid state, compounds **3a**−**3d** are very stable and can be stored at room temperature without any observable decomposition for months. However, a change in color was observed upon treating the solutions of **3a**−**3d** with acid. The resulting decompositions of **3a**−**3d** were then studied spectrophotometrically in a phosphate buffer at pH 5.0. The decay of absorbance for each compound was monitored. Using the same initial concentrations, each of the compounds exhibited varying decay rates with half-lives of approximately 1, 6, 15, and 130 min for **3a**, **3b**, **3c**, and **3d**, respectively (Figure 2). Compound **3d** with an electron-donating group (−OCH_3) was more stable as compared to the unsubstituted **3b**, or **3a** with an electron-withdrawing substituent (−CF_3). The dependence of the decay rate within the pH range of 5.0−7.0 was also investigated for a representative compound, **3b** (Figure 3). As shown in Figure S2 of the Supporting Information, the rate of decay for **3b** increases with decreasing pH with calculated first-order rate constants of k = 0.005, 0.03, 0.06, 0.13, and 0.24 min^{-1} at pH 7.0, 6.5, 6.0, 5.5, and 5.0, respectively. This result further indicates that the decomposition of aryloxathiazolyliumolates is acid-catalyzed.

In solution, the decomposition of **3b** in the presence of stray light was also monitored and only showed that 7% of the original amount decomposed over a period of 3 h. The decomposition of **3b** is slower as compared to *S*-nitrosoglutathione (GSNO) with 21% of the compound that decomposed over the same period of time (Figure S3 of the Supporting Information). This result indicates that aryloxathiazolyliumolates are relatively more stable as compared to RSNO in aqueous solution at ambient conditions. In acetonitrile, all of the aryloxathiazolyliumolates were found to be stable with only minimal decomposition after 2 h at 37 °C (Figure 4).

Detection of Nitric Oxide. To verify if the decomposition pathway for **3a**−**3d** did involve NO release (Scheme 3), electron paramagnetic resonance (EPR) spin trapping was used to directly detect NO. The detection of NO was carried out using two methods: (1) purging the acidified solution of **3a**−**3d** with argon and allowing the gas to pass through the [$(MGD)_2$−Fe^{II}] spin trap solution;[47] and (2) directly mixing the acidified solution of **3a**−**3d** with [$(MGD)_2$−Fe^{II}].[48] For both techniques, a triplet signal with g_{iso} = 2.041 and hyperfine splitting constant (hfsc) of a_N = 12.70 G (lit. g_{iso} = 2.04 and a_N = 12.70 G)[49] as well as line width of ΔB_{pp} = 3.32 G were observed (Figure 5a). This spectral feature is consistent with the formation of an [$(MGD)_2$−Fe^{II}−NO] adduct when SNAP was used as the standard at the same pH of 5 (Figure 5b). The low EPR signal intensity observed for the [$(MGD)_2$−Fe^{II}−NO] adduct, despite the already high concentration of [$(MGD)_2$−Fe^{II}] used of 20 mM, could be due to the weaker basicity of NO in the presence of an acid because competition between the two Lewis acids (i.e., the proton and Fe^{2+}) for NO can occur in solution. Heating the acidified mixture containing the [$(MGD)_2$−Fe^{II}] to 45 °C for 10 min increased the intensity of the EPR signal 2-fold. This increase in signal intensity at elevated temperature could be due to the faster decomposition of compounds **3a**−**3d**. There was no evidence of [$(MGD)_2$−Fe^{II}−NO] formation at neutral pH, indicating that NO production from **3a**−**3d** is initiated by acid. The formation of [$(MGD)_2$−Fe^{II}−NO] adduct was also observed in the CH_3CN−water (1:9) solvent system.

The formation and decay of [$(MGD)_2$−Fe^{II}−NO] was monitored by EPR (Figure 6). The low-field peak intensity was monitored over a period of 13 min using the direct mixing technique at pH 5.0 and 7.0. The formation of [$(MGD)_2$−Fe^{II}−NO] was instantaneous after acidification of the mixture containing **3a**−**3d** and [$(MGD)_2$−Fe^{II}], and then the signal intensity gradually decays. Using the same concentration (i.e, 20 mM) for all compounds, different maxima for **3a**−**3d** were

(45) Bruce, J. M.; Sutcliffe, F. K. *J. Chem. Soc. Abstr.* **1957**, 4789.
(46) Gotthardt, H. *Chem. Ber.* **1972**, *105*, 188.
(47) Li, H.; Cui, H.; Liu, X.; Zweier, J. L. *J. Biol. Chem.* **2005**, *280*, 16594.
(48) Mordvintcev, P.; Muelsch, A.; Busse, R.; Vanin, A. *Anal. Biochem.* **1991**, *199*, 142.
(49) Xia, Y.; Cardounel, A. J.; Vanin, A. F.; Zweier, J. L. *Free Radical Biol. Med.* **2000**, *29*, 793.

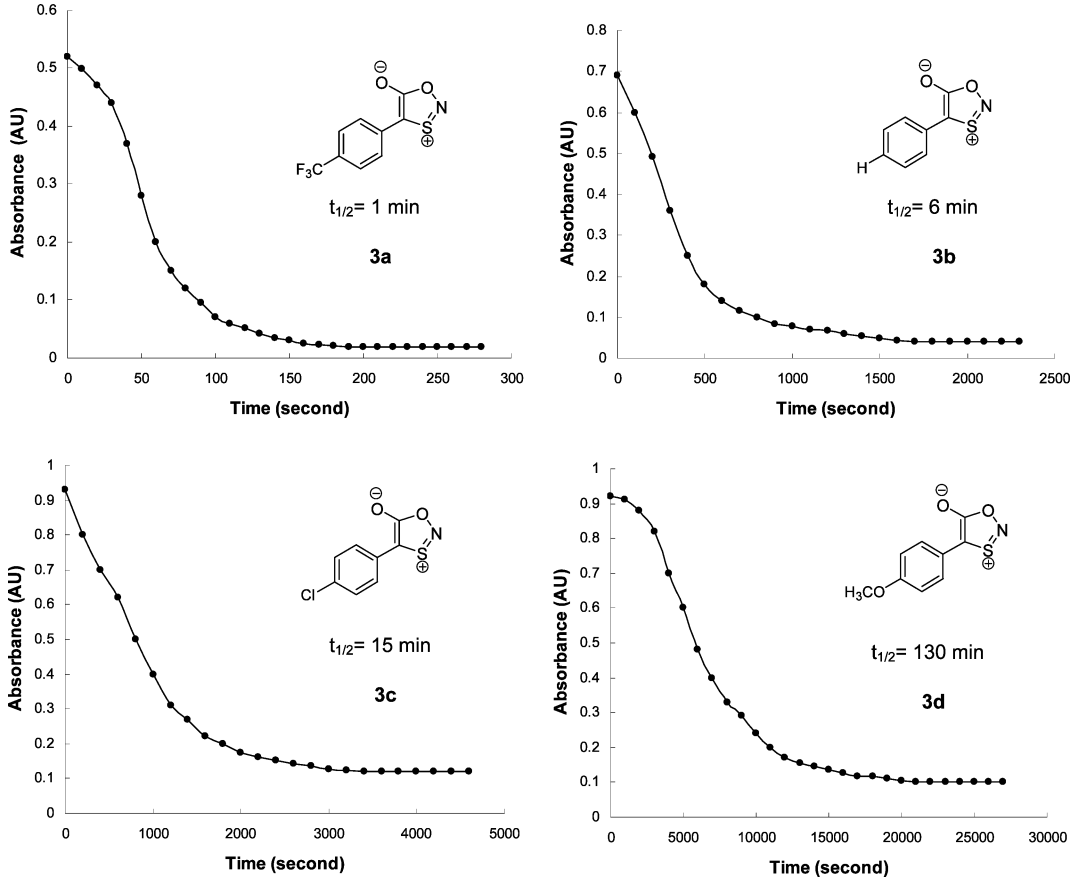

Figure 2. Decomposition of **3a**−**3d** (0.8 mM) in 0.1 M phosphate buffer, pH 5.0, 37 °C. UV was measured at 581 nm (**3a**), 587 nm (**3b**), 592 nm (**3c**), and 602 nm (**3d**).

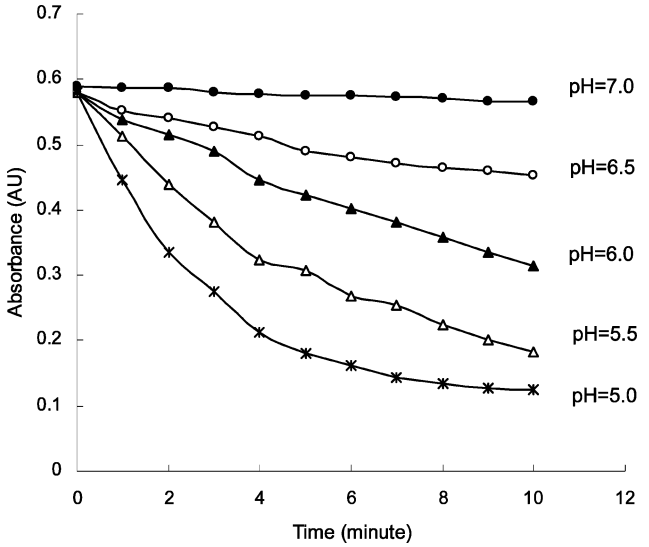

Figure 3. Decomposition plot at 587 nm of **3b** (0.4 mM) in 0.1 M phosphate at pH 5.0−7.0.

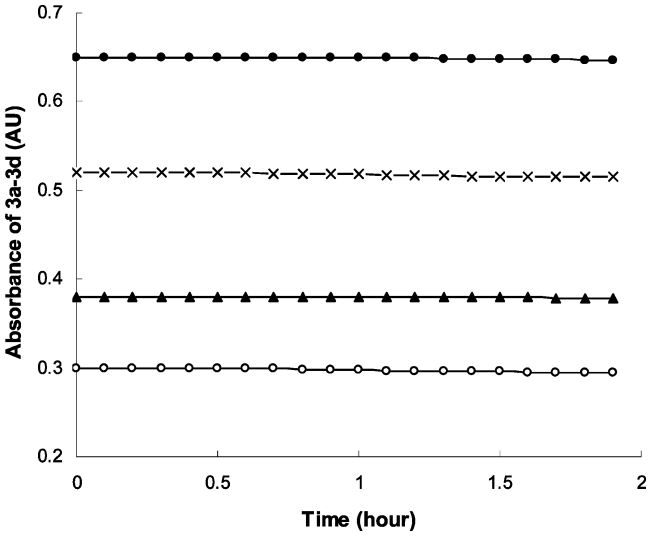

Figure 4. Decompositions of **3a** (○), **3b** (●), **3c** (▲), and **3d** (×) (0.4 mM, in acetonitrile, 37 °C). Absorbance was measured at 581 nm (**3a**), 587 nm (**3b**), 592 nm (**3c**), and 602 nm (**3d**).

observed using SNAP as standard, assuming that 99.9% of NO was released from SNAP at pH 5. A concentration of 5.34 mM of [$(MGD)_2$−Fe^{II}−NO] was achieved for **3a**, which corresponds to ∼27% total NO, while the lowest NO concentration was observed for **3d** (∼9% yield). No evidence of [$(MGD)_2$−Fe^{II}−NO] formation was observed at pH 7.0. Because the unsubstituted aryloxathiazolyliumolates (**3b**) have an NO yield of 21%, these results show that the presence of an electron-withdrawing substituent at the para position of the aryl group (**3a**) enhances the NO-releasing property of the aryloxathiazolyliumolates, whereas the electron-donating substituent decreases it. This substituent effect can be exploited as a means to "fine-tune" the NO-releasing property of aryloxathiazolyliumolates.

Detection of Thiyl Radical Intermediates. We propose that there is a formation of a thiyl radical when NO is released via the homolytic S−N bond cleavage as has been found in the decomposition pathway for many RSNO compounds.[50] However, the heterolytic bond cleavage of S−N to form nitroxyl

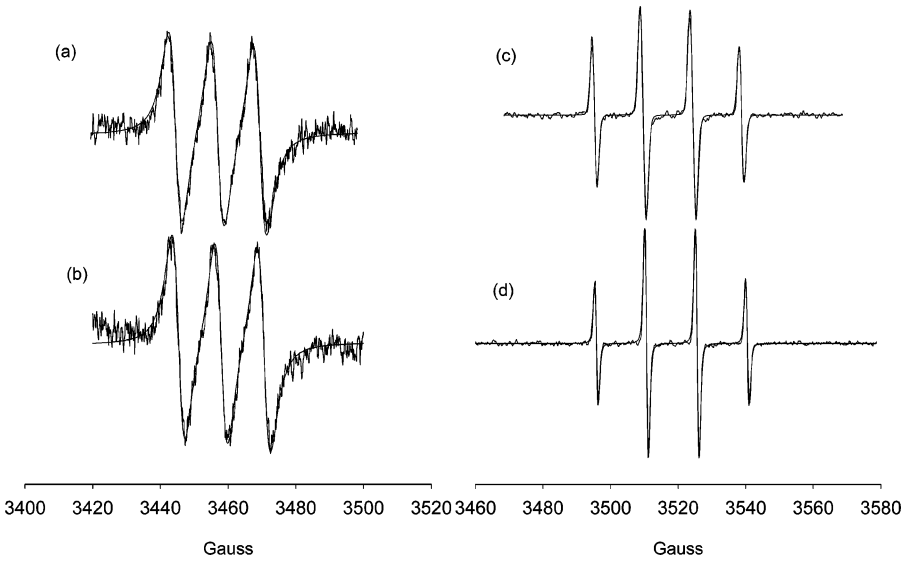

Figure 5. X-band EPR and simulated (overlapped) spectra of (a) NO-adduct arising from **3a** (20 mM) in the presence of [$(MGD)_2$−Fe^{II}] (20 mM), a_N = 12.70 G, ΔB_{pp} = 3.32 G; (b) NO-adduct arising from SNAP (6 mM) in the presence of [$(MGD)_2$−Fe^{II}] (20 mM), a_N = 12.64 G, ΔB_{pp} = 3.35 G; (c) S-centered spin adduct arising from DMPO (200 mM) and **3a** (20 mM) all at pH 5, a_N = 14.74 G, a_H = 13.92 G, ΔB_{pp} = 0.78 G; (d) hydroxyl radical adduct from UV photolysis of 0.5% H_2O_2 in the presence of 25 mM DMPO, a_N = 14.97 G, a_H = 14.73 G, ΔB_{pp} = 0.59 G.

Scheme 3. Radical−Radical Reactions for the Decomposition of **3a**−**3d** upon Acidification[a]

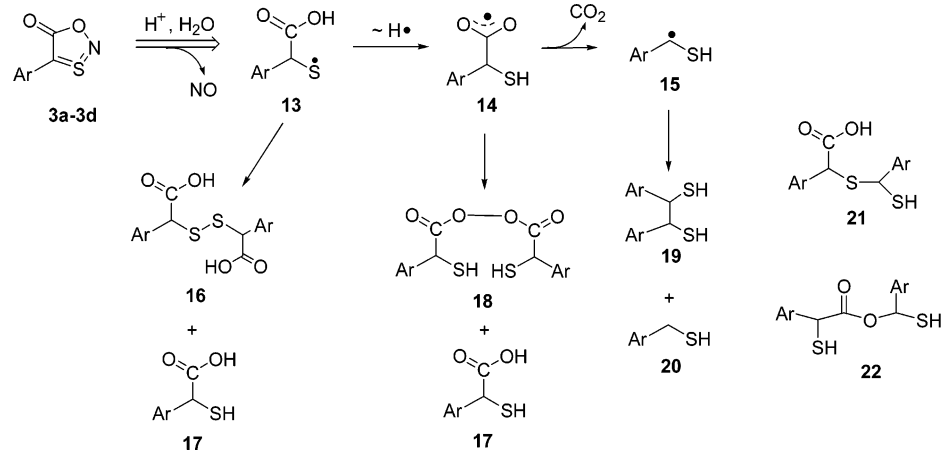

[a] Compounds **4**−**12** are part of the decomposition mechanism as shown in Tables 3 and 4.

(NO^-) might also be possible, because the [$(MGD)_2$−Fe^{II}−NO] adduct can form from NO^- and [$(MGD)_3$−Fe^{III}]. EPR spin trapping was used to detect any other radical intermediates formed other than NO to determine which type of S−N cleavage was responsible for the release of NO. Figure 5c shows a typical EPR spectrum obtained upon the acidification of compound **3a** in the presence of a nitrone spin trap, DMPO. The observed overall hyperfine feature of 1:2:2:1 is similar to that found for the DMPO−OH adduct (Figure 5d). However, the spectral profile was significantly different for DMPO−**3a** adduct with hfsc's of a_N = 14.74 G and a_H = 13.92 G, as compared to the DMPO−OH adduct with a_N = 14.97 G and a_H = 14.73 G (lit. a_N = 14.9 G and a_H = 14.9 G).[51] Moreover, the observed peak-to-peak line width in Figure 5c is much broader with ΔB_{pp} = 0.78 G as compared to DMPO−OH's ΔB_{pp} = 0.59 G (Figure 5d). Furthermore, the DMPO spin adducts arising from the acidification of compounds **3b**, **3c**, and **3d** gave EPR spectra with hfsc's that are different from **3a**, for example, for **3b**, a_N = 14.30 G and a_H = 15.31 G; **3c**, a_N = 14.29 G and a_H = 15.32 G; and **3d**, a_N = 14.29 G and a_H = 15.26 G. All of the EPR spectra from the DMPO adducts of **3b**−**3d** gave line widths similar to that of **3a** with ΔB_{pp} = 0.70−0.73 G. The observed EPR parameters were further supported by the EPR spectral parameters reported for S-centered radicals generated from low molecular weight thiols whose hfsc values were in the range of a_N = 15.2−15.8 G and a_H = 15.2−18.0 G.[52] The differences in the EPR spectral parameters between DMPO−OH and the spectra arising from the decomposition of **3a**−**3d** in the presence of DMPO indicate the formation of a radical other than HO•.

To further confirm the nature of the radical generated from **3**, the spin trap α-phenyl-*tert*-*N*-butyl nitrone (PBN) was also employed for the detection of thiyl intermediates by EPR. Using the Fenton system, the PBN−OH adduct was generated giving the following hfsc's: a_N = 14.43 G and a_H = 2.42 G,[53] a_N = 14.76 G and a_H = 2.75 G. However, acidification of **3b** solution

(50) Wang, P. G.; Xian, M.; Tang, X.; Wu, X.; Wen, Z.; Cai, T.; Janczuk, A. J. *Chem. Rev.* **2002**, *102*, 1091.
(51) Villamena, F. A.; Hadad, C. M.; Zweier, J. L. *J. Phys. Chem. A* **2003**, *107*, 4407.
(52) Davies, M. J.; Forni, L. G.; Shuter, S. L. *Chem. Biol. Interact.* **1987**, *61*, 177.
(53) Hinton, R. D.; Janzen, E. G. *J. Org. Chem.* **1992**, *57*, 2646.

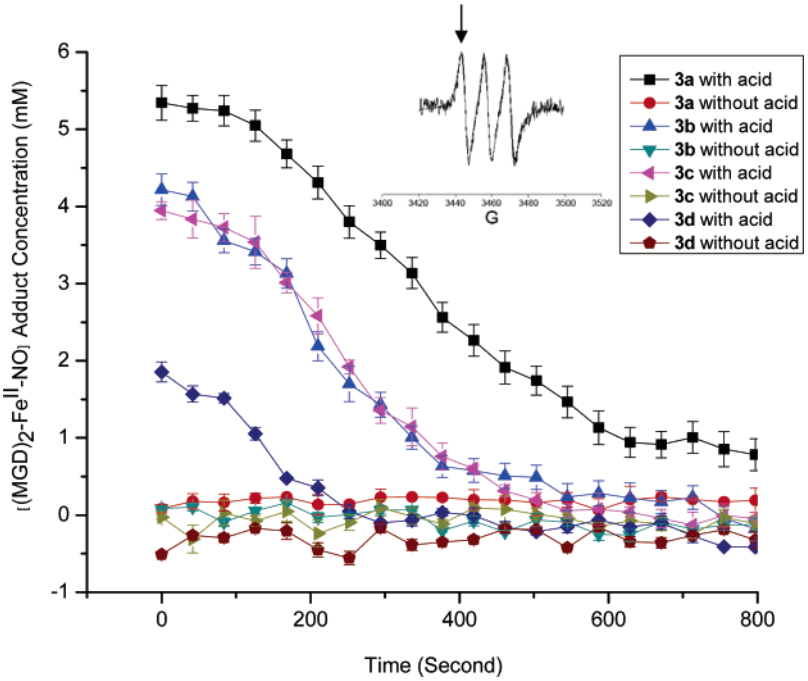

Figure 6. Formation and decay of [(MGD)$_2$−Fe^{II}−NO] adduct generated from **3a**−**3d** (20 mM) in the presence of [(MGD)$_2$−Fe^{II}] (20 mM) at pH 5.0 and 7.0. The arrow indicates the peak that is being monitored. All data were the average of three measurements with a standard deviation of less than 10%.

Table 1. ESI Mass of Various Products Generated from the Acidification of Aryloxathiazolyliumolate **3a**[a]

product	**16** or **18**	**17**	**19**	**20**	**21** or **22**
M_{obs}	471.7	not observed	383.7	191.6	427.1
M_{calcd}	471.4	237.2	383.4	193.2	427.4
M + Na$_{obs}$	493.5	259.2	407.4	not observed	449.5
M + Na$_{calcd}$	493.4	259.2	405.4	215.2	449.4

[a] Refer to Scheme 3 for the respective structures.

Table 2. Reduction Potentials $E_{1/2}$ of **3a**−**3d** Determined by Cyclic Voltammetry Relative to Ag/AgCl in 1 mM $TBABF_4$ Acetonitrile

compound	$E_{1/2}$ (red$_1$) (V)	$E_{1/2}$ (red$_2$) (V)	$E_{1/2}$ (red$_3$) (V)
3a	−0.56	−1.05	−1.56
3b	−0.65	−1.19	−2.40
3c	−0.66	−1.14	−1.56
3d	−0.67	−1.19	−2.48

in the presence of PBN gave hfsc's of a_N = 14.33 G and a_H = 2.05 G, which are similar to those observed for the spin trapping of low molecular weight thiyl radicals by PBN with hfsc's of a_N = 14.46 G and a_H = 1.53−2.09 G.[54] Therefore, the radical generated during acidification of aryloxathiazolyliumolates is most probably an S-centered radical. Even though there is also the possibility that an O-centered adduct is formed, an H-atom migration is not likely to occur due to the endoergic nature of this reaction (Table 4, reaction V).

No radical formation was observed at neutral pH using DMPO as a spin-trap similar to when [(MGD)$_2$−Fe^{II}] was used (Figure 7). The DMPO spin adduct formation from **3a**−**3d** was quantified using a stable nitroxide, 3-CP, and is shown in Figure 6. The growth of the first low-field peak was monitored over a period of 20 min. At the initial concentration of 20 mM, the maximum concentration of DMPO−adduct formed from **3a** is the highest (6.5 mM) as compared to the amount of adduct formed from **3b**−**3d** with **3d** giving the least amount of adduct formed (0.84 mM). This preference of DMPO adduct formation follows the same qualitative trend as observed for the NO adduct formation. This further supports the electronic effect of the aryl substituents on the radical generating ability of the aryloxathiazolyliumolate analogues.

The difference in the formation profile between Figures 5 and 6 for the spin adducts using [(MGD)$_2$−Fe^{II}] and DMPO, respectively, could be due to the fast rate of formation of the [(MGD)$_2$−Fe^{II}−NO] adduct with $k \approx 10^8$ M^{-1} s^{-1} [55] as compared to the formation of the S-centered radical adduct with DMPO, which was shown to be reversible with $k \approx 10^7$−10^8 M^{-1} s^{-1}.[56,57]

Mass Spectral Analysis. Electrospray ionization (ESI) mass spectrometric analysis of the decomposition products from the acidified **3a** was carried out to confirm the generation of the radical intermediates. Product analysis of **3a** before acidification only yielded the parent ions of compound **3a**; however, upon treatment with an acid a variety of products were produced, which is indicative of radical−radical reaction as shown in Scheme 3 and Table 1. Based on Scheme 3, dimerization of intermediates **13** or **14** yielded either compound **16** or **18**, which lends support to the observed mass at 471.7 *m*/*z*. The observed mass of 427.1 *m*/*z*, which corresponds to the products **21** or **22**, is evident of a mixed radical−radical reaction of intermediates **13** or **14** with **15**. H-atom abstraction by the radicals **13**, **14**, and **15** gave compounds **17** and **20** and is consistent with the observed masses at 259.2 *m*/*z* (M + Na) and 191.6 *m*/*z*, respectively. Evidence of dimer **19** formation from the radical intermediate **15** was observed with mass of 383.7 *m*/*z*. These analyses reveal the formation of radical intermediates during the decomposition path.

(54) Ionita, P.; Gilbert, B. C.; Whitwood, A. C. *Lett. Org. Chem.* **2004**, *1*, 70.
(55) Fujii, S.; Yoshimura, T. *Coord. Chem. Rev.* **2000**, *198*, 89.
(56) Davies, M. J.; Forni, L. G.; Shuter, S. L. *Chem. Biol. Interact.* **1987**, *61*, 177.
(57) Potapenko, D. I.; Bagryanskaya, E. G.; Tsentalovich, Y. P.; Reznikov, V. A.; Clanton, T. L.; Khramtsov, V. V. *J. Phys. Chem. B* **2004**, *108*, 9315.

Table 3. Aqueous Phase Reaction Enthalpies ($\Delta H_{298K,aq}$) and Free Energies ($\Delta G_{298K,aq}$) for Various Steps Leading to the Formation of RSNO at the PCM/B3LYP/6-31+G**//B3LYP/6-31G* Level in kcal/mol

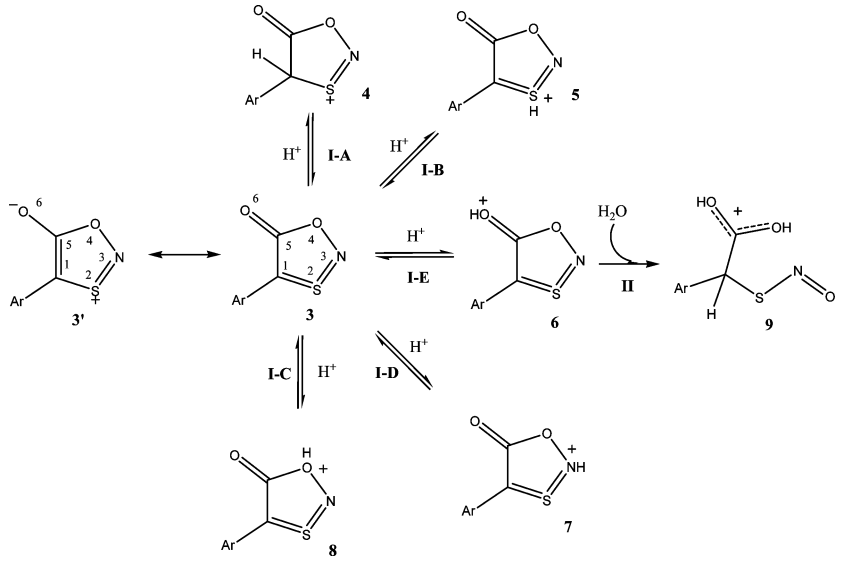

	$\Delta H_{298K,aq}$						$\Delta G_{298K,aq}$					
	I-A	I-B	I-C	I-D	I-E	II	I-A	I-B	I-C	I-D	I-E	II
3a ($-CF_3$)	8.9	20.5	16.2	−7.6	−9.7	−5.1	9.0	17.5	14.8	−7.3	−8.8	−8.6
3c ($-Cl$)	8.1	19.9	15.4	−11.1	−10.7	−4.7	8.0	16.8	13.9	−10.7	−10.1	−8.3
3b ($-H$)	6.4	18.9	14.6	−12.0	−11.6	−4.1	6.3	16.0	13.1	−11.6	−10.8	−7.7
3d ($-OCH_3$)	7.2	14.9	14.9	−16.7	−12.1	−3.3	7.6	37.9	13.7	−16.2	−11.3	−6.9

Table 4. Aqueous Phase Reaction Enthalpies ($\Delta H_{298K,aq}$) and Free Energies ($\Delta G_{298K,aq}$) for Various Steps after the Release of NO at the PCM/B3LYP/6-31+G**//B3LYP/6-31G* Level in kcal/mol

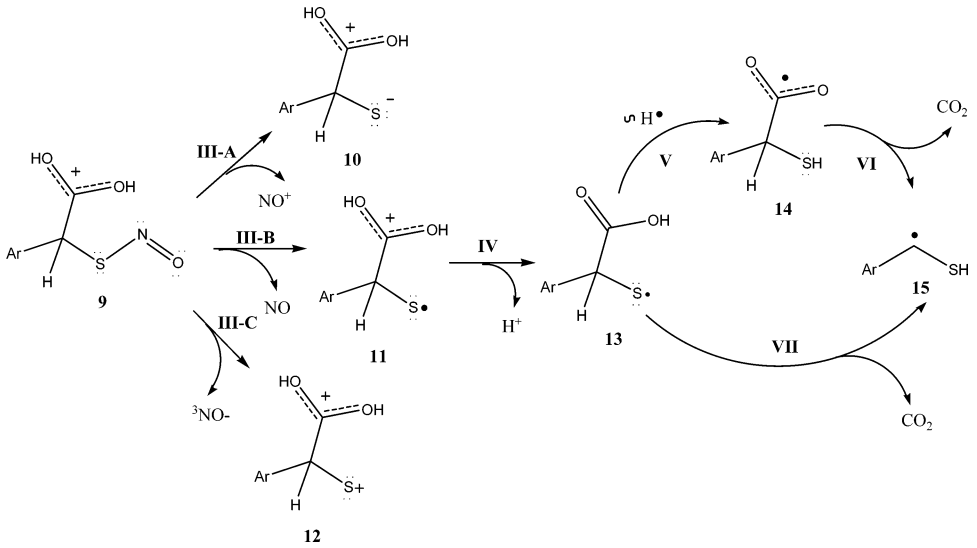

	$\Delta H_{298K,aq}$							$\Delta G_{298K,aq}$						
	III-A	III-B	III-C	IV	V	VI	VII	III-A	III-B	III-C	IV	V	VI	VII
3a ($-CF_3$)	42.2	32.4	69.6	3.2	9.5	−22.9	−13.4	31.5	20.5	57.6	2.3	8.3	−33.2	−24.9
3c ($-Cl$)	43.5	32.1	59.8	3.9	8.3	−20.2	−11.8	32.8	20.5	48.2	3.9	7.2	−31.2	−23.9
3b ($-H$)	44.2	31.5	59.7	1.3	11.7	−19.5	−7.8	33.6	19.9	48.1	1.2	10.9	−30.1	−19.3
3d ($-OCH_3$)	44.7	30.9	46.8	4.2	6.8	−15.5	−8.8	34.2	19.6	35.1	4.2	5.7	−26.2	−20.5

Reducibility of Aryloxathiazolyliumolates. The decomposition of **3a** in the presence of two common bioreductants,[58,59] L-ascorbic acid or reduced L-(−)-glutathione, was measured spectrophotometrically. Because no change in the absorption profile before and after the addition of the reductants was observed, it can be concluded that **3a** is stable in the presence of these reductants. This observation was further confirmed

(58) Halliwell, B.; Gutteridge, J. M. C. *Free Radicals in Biology and Medicine*, 3rd ed.; Oxford University Press, Inc.: New York, 1999.
(59) Buettner, G. R. *Arch. Biochem. Biophys.* **1993**, *300*, 535.

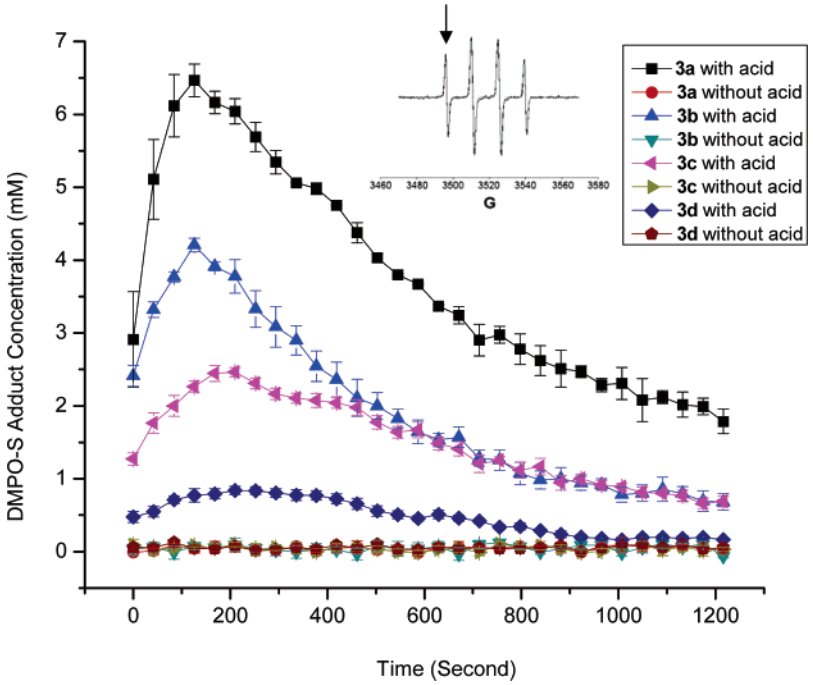

Figure 7. Formation and decay of S-centered DMPO adduct generated from **3a**−**3d** (20 mM) in the presence of DMPO (200 mM) at pH 5.0 and 7.0. Arrow indicates the peak that is being monitored. All data were the average of three measurements. The reproducibility of peak intensities is reasonable with a standard deviation of less than 10%.

using EPR spin trapping, which did not show any radical adduct formation when L-ascorbic acid or reduced L-(−)-glutathione was introduced into the solution containing **3a** and DMPO. Both results from spectrophotometric and EPR experiments are consistent with the reduction potential observed for **3a** using cyclic voltammetry as shown in Table 2. The observed first reduction ($E_{1/2}$) for **3a** of −0.56 V is higher as compared to those found for ascorbate and glutathione of −0.28[58] and −0.26 V,[60] respectively (the literature $E_{1/2}$ values for other RSNO's are −0.80 to −1.14 V).[61] The observed reduction potentials for **3b**−**3d** range from −0.65 to −0.67 V, and, therefore, this series of aryloxathiazolyliumolates (**3a**−**3d**) exhibit relative stability in the presence of bioreductants. Stability in the presence of metal ion was also explored, and results show that **3b** (0.4 mM) in the presence of 10 μM Fe^{2+} decomposed to about 16% over a period 20 min, and this rate of decomposition is similar to that of using GSNO (0.8 mM) in the presence of 20 μM Fe^{2+} (Figure S4 of the Supporting Information).

Computational Results. Over the last 15 years, many different decomposition pathways of RSNOs have been reported such as unimolecular homolytic cleavage, metal-catalyzed, and photolytic processes.[62] However, it has been accepted that the decomposition pathway is highly dependent on the reaction conditions, while the factors that determine their stability in solution are not yet fully understood.[63] Nevertheless, ongoing research has added to our understanding of the chemistry of nitrosothiols; most recently, for example, a pathway has been proposed where decomposition is catalyzed by nitrosonium.[62]

Based on our experimental evidence, aryloxathiazolyliumolate compounds are relatively stable at neutral pH and NO is produced only upon treatment with acid. Furthermore, our results also suggest that the decomposition of aryloxathiazolyliumolate is acid-catalyzed as shown in Figure 3 and that their NO-releasing property is influenced by the substituents on the aryl moiety. This computational study has two goals: (1) to determine a plausible mechanism for the decomposition of aryloxathiazolyliumolates; and (2) to determine whether aryl substitution by electron-donating or electron-withdrawing groups has an effect on the favorability of decomposition of aryloxathiazolyliumolates. The PCM/B3LYP/6-31+G**//B3LYP/6-31G* level of theory that takes into account the solvation effect of water was employed. It has been reported that the B3LYP density functional theory method overestimates S−N bond lengths by 0.5−0.1 Å, and, therefore, the activation energies obtained are lower than they should be.[64] Nevertheless, we chose this level of theory to achieve the best compromise between computational cost and accuracy due to the size of our molecules and the consideration of solvation effects in the calculation.

In this study, only the probable stable intermediates have been calculated, and thus the values in Table 3 only represent the favorability in reaction free energies (ΔG). Based on the assumption that the decomposition of **3** occurs after introduction of H^+, then protonation of **3** should be the first step to the decomposition pathway and should also be energetically favorable (see Table 3).

Optimization of aryloxathiazolyliumolates (**3′**) gave a structure with C−O bond length of 1.21 Å similar to those found in esters with a C═O bond of 1.23 Å. It is, therefore, reasonable to assume that the starting structure resembles that of lactone compounds (see structure **3**, Table 3). The favorability of protonation on five possible sites of the pentacylic ring was

(60) Millis, K. K.; Weaver, K. H.; Rabenstein, D. L. *J. Org. Chem.* **1993**, *58*, 4144−6.
(61) Hou, Y.; Wang, J.; Arias, F.; Echegoyen, L.; Wang, P. G. *Bioorg. Med. Chem. Lett.* **1998**, *8*, 3065.
(62) Zhao, Y.-L.; McCarren, P. R.; Houk, K. N.; Choi, B. Y.; Toone, E. J. *J. Am. Chem. Soc.* **2005**, *127*, 10917.
(63) de Oliveira, M. G.; Shishido, S. M.; Seabra, A. B.; Morgon, N. H. *J. Phys. Chem. A* **2002**, *106*, 8963.
(64) Baciu, C.; Gauld, J. W. *J. Phys. Chem. A* **2003**, *107*, 9946.

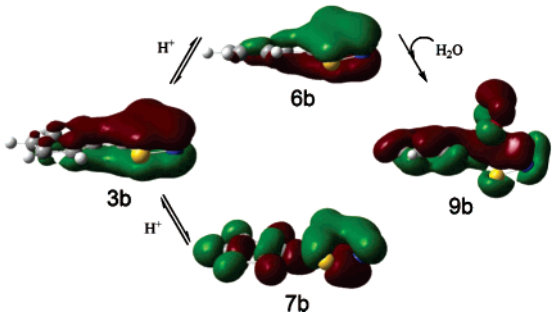

Figure 8. Lowest energy molecular orbitals of **3b**, **6b**, **7b**, and **9b** (red lines) calculated at 6-31+G** in Gaussian 03 to show the π electron delocalization between the aryl and pentacyclic ring systems and its subsequent disruption upon hydration.

investigated (i.e., C-1, S-2, N-3, O-4, and O-6). Table 3 shows that the protonations at the benzylic C-1 (reaction I-A), ester O-4 (reaction I-C), and S-2 (reaction I-B) were all endoergic by ~7, ~14, and ~17 kcal/mol, respectively. Protonation on the carbonyl O-6 (reaction I-E) or N-3 (reaction I-D) was found to be exoergic by 7−16 kcal/mol. These results correlate with the natural bond orbital (NBO) analysis[65] of the charges on the relevant atoms of the pentacyclic SNO of **3a**−**d** showing the highest charge density on the carbonyl O-6 with −0.65 e followed by the benzylic C-1 (−0.36 e to −0.38 e), N-3 (−0.32 e to −0.36 e), and O-4 (−0.33 e to −0.34 e) with S-2 being the most positive with a charge density of 0.88 e−0.92 e. It is also interesting to note that the endoergic protonation on C-1, O-4, and S-2 resulted in the opening of the pentacyclic ring, while this was not observed upon protonation at O-6 and N-3. Because the energetics of protonation at the O-6 and N-3 are almost the same and no pentacyclic ring opening occurred, it can be assumed that both of the protonated species, **6** and **7**, could exist in solution. Molecular orbital analyses of the starting molecules **3a**−**d** showed π electron conjugation between the pentacyclic SNO ring and the aryl system (see Figure 8 for **3b**). Because of this extensive π electron delocalization between the two ring systems, the aryl substituents can exert an electronic effect on the pentacyclic ring. Both the O-6 and the N-3 protonation follow a trend that is consistent with the electron-donating or -withdrawing capabilities of the aryl substituents: ease of protonation follows $-OCH_3 > -H > -Cl > -CF_3$. Moreover, the π electron conjugation is conserved upon protonation of the carbonyl O to yield compounds **6a**−**d**.

We hypothesize that the mechanism for decomposition of **6a**−**d** would resemble that of ester hydration, where the rate-determining step would be the hydration step.[66] Because of the high positive charge density on the C-5 atom (0.73 e) (see Table 3, reaction II), the most favorable site for nucleophilic addition of H_2O to compounds **6a**−**d** is at the C-5 position to give **9a**−**d**. Reaction II shows pentacyclic ring opening with loss of π electron conjugation on **9a**−**d** with exoergic free energies of reaction ($\Delta G_{298K,aq}$) that range from −6.9 to −8.6 kcal/mol. Substituent effect has also been observed for reaction II with the $-CF_3$ compound being the most susceptible to water addition, and $-OCH_3$ being the least susceptible.

The overall $\Delta G_{298K,aq}$ values (reaction IE + reaction II) are (in kcal/mol): −17.4 (**3a**), −18.5 (**3b**), −18.4 (**3c**), and −18.2 (**3d**) and may not reflect the relative rates of reaction as observed experimentally. Calculation of activation energy barriers ($\Delta G^{\ddagger}$) for reactions IE and II would have provided a more definitive trend on the relative rates of hydrolysis. Nevertheless, the overall exoergic $\Delta G_{298K,aq}$ values suggest that reactions IE and II are the most preferred pathways for the decomposition of **3** under acidic condition.

Shown in Table 4 are the enthalphies and free energies of NO release from the hydrated aryloxathiazolyliumolates (reaction III-B) with $\Delta H_{298K,aq}$ values of 30.9−32.4 kcal/mol close to the reported[63,64,67] S−N bond dissociation energies of ~30 kcal/mol for RSNOs with a benzyl group or a non-conjugated alkyl system. The free energies ($\Delta G_{298K,aq}$) of 19.6−20.5 kcal/mol for NO release from compounds **9a**−**d** were found to be similar to those reported for related RSNO compounds with values of 20−22 kcal/mol.[64,68−70] The small differences in free energies of reaction for step III-B (~1 kcal/mol) indicate that the substituents may have little effect on the favorability of NO release from the hydrated compounds **9a**−**d**.

The favorability of heterolytic S−N bond cleavage to form the nitrosonium cation (NO^+) (reaction III-A) and the ground triplet nitroxyl ($^3NO^-$) (reaction III-C) from **9a**−**d** was also computationally explored to determine whether a more energetically favorable pathway exists for the decomposition of **9a**−**d**. Results indicate, however, that the formation of NO^+ and $^3NO^-$ from **9a**−**d** is more endoergic as compared to the formation of NO via homolytic cleavage (reaction III−B). The decomposition pathways following release of NO (reactions V−VII) show that the release of CO_2 via reaction VII is the most preferred path for the final product formation. The formation of the radical **15** is further supported by product analysis using MS (Scheme 3, Table 1) as mentioned previously.

Vasodilation Studies. The ability of the aryloxathiazolyliumolate compounds to induce NO-dependent vasodilation was investigated using rat aortic rings. Rings were stretched to generate a resting tension of 1 g and allowed to equilibrate for 20 min. Following the equilibration period, the vessels were constricted with phenylephrine (0.5 μM), and the relaxation response to the aryloxathiazolyliumolate compounds was measured. The % relaxation was then compared among the drug-treated groups. These results demonstrated that exposure to compounds **3a**−**3d** resulted in a pH-dependent relaxation with maximal effects observed at pH 6.0 exhibiting 59%, 35%, 63%, and 71% relaxation, respectively (Figure 9). The relaxation response was significantly less pronounced at pH 7.4, in which 16%, 8%, 37%, and 44% relaxation was observed. These results demonstrate that the aryloxathiazolyliumolates have biological activity, and upon NO release induce vascular relaxation. The pH dependence of the relaxation response is consistent with our previous results demonstrating enhanced NO release in acidic environments.

Experimental Section

General Procedures. All reagents were purchased from commercial sources and used without further purification. ^1H NMR and ^{13}C NMR

(65) Reed, A. E.; Curtiss, L. A.; Weinhold, F. *Chem. Rev.* **1988**, *88*, 899.
(66) Bender, M. L. *Chem. Rev.* **1960**, *60*, 53.
(67) Lue, J.-M.; Wittbrodt, J. M.; Wang, K.; Wen, Z.; Schlegel, H. B.; Wang, P. G.; Cheng, J.-P. *J. Am. Chem. Soc.* **2001**, *123*, 2903.
(68) Arulsamy, N.; Bohle, D. S.; Butt, J. A.; Irvine, G. J.; Jordan, P. A.; Sagan, E. *J. Am. Chem. Soc.* **1999**, *121*, 7115.
(69) Grossi, L.; Montevecchi, P. C. *Chem.-Eur. J.* **2002**, *8*, 380.
(70) Toubin, C.; Yeung, D. Y. H.; English, A. M.; Peslherbe, G. H. *J. Am. Chem. Soc.* **2002**, *124*, 14816.

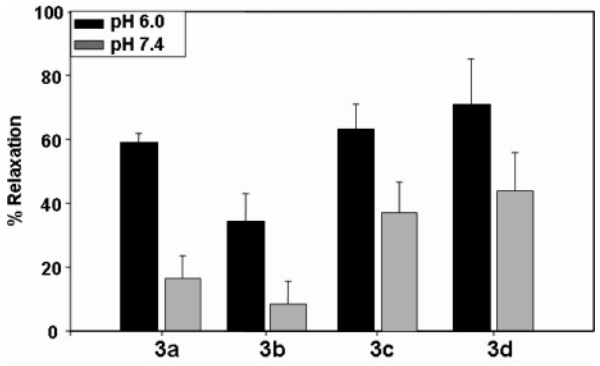

Figure 9. Vasodilation effects of 20 μM of **3a**−**3d** at pH 6.0 and 7.4.

spectra were recorded on a 400 MHz spectrometer. Chemical shifts (δ) are given in ppm relative to tetramethylsilane (TMS) as internal standard. Silica gel plates (Merck F254) and silica gel 60 (Merck, 70−230 mesh) were used for thin-layer chromatography (TLC) and column chromatography, respectively. Molecular weight was verified using an ESI mass spectrometer.

General Synthesis of *S*-Acetyl-α-aryl-α-mercaptoacetic Acids (2a−2d). A mixture of compound **1a**, **1b**, **1c**, or **1d** (10 mmol) and thiolacetic acid (20 mmol) in THF (25 mL) was added dropwise to a stirred THF solution (50 mL) of the preformed adduct of triphenyl phosphate (20 mmol) and diisopropyl azodicarboxylate (20 mmol) at 0 °C. After the addition was completed, the mixture was stirred at 0 °C until the solution turned clear. The ice bath was removed, and stirring was continued for 1 h at room temperature. The solution was evaporated, and the residue was dissolved in CH_2Cl_2 (50 mL) and extracted twice with 1 M $NaHCO_3$ solution (30 mL). The basic aqueous layer was washed with CH_2Cl_2 (20 mL × 3). The aqueous layer was acidified with 12 M HCl to pH ≈ 3, and then extracted with CH_2Cl_2 (20 mL × 3). The combined organic layers were dried over $MgSO_4$, and the solvent was evaporated.

***S*-Acetyl-α-(*p*-trifluoromethylphenyl)-α-mercaptoacetic Acid (2a).** The crude product **2a** (2.27 g, 8.17 mmol, yield 82%) was obtained and used for the deprotection without further purification. ^{1}H NMR (500 MHz, $CDCl_3$): δ 10.71 (brs, 1H), 7.59 (d, J = 8.3 Hz, 2H), 7.51 (d, J = 8.3 Hz, 2H), 5.35 (s, 1H), 2.36 (s, 3H). ^{13}C NMR (125 MHz, $CDCl_3$): δ 193.1, 174.7, 138.3, 130.9 (q, J = 32.8 Hz), 129.0, 125.9 (q, J = 3.6 Hz), 123.7 (q, J = 272.3 Hz), 50.2, 30.0. HRMS (M + Na^+) (ESI) calcd for $C_{11}H_9F_3O_3SNa^+$ 301.0122, found 301.0120.

***S*-Acetyl-α-phenyl-α-mercaptoacetic Acid (2b).** The crude product **2b** (1.68 g, 8.0 mmol, yield 80%) was directly used for the deprotection without further purification. ^{1}H NMR (400 MHz, $CDCl_3$): δ 10.28 (brs, 1H), 7.41−7.32 (m, 5H), 5.31 (s, 1H), 2.36 (s, 3H). ^{13}C NMR (100 MHz, $CDCl_3$): δ 194.0, 175.7, 134.2, 129.1, 128.9, 128.7, 51.0, 30.1. HRMS (M + Na^+) (ESI) calcd for $C_{10}H_{10}O_3SNa^+$ 233.0248, found 233.0247.

***S*-Acetyl-α-(*p*-chlorophenyl)-α-mercaptoacetic Acid (2c).** Compound **2c** (1.76 g, 7.2 mmol, yield 72%) was obtained as a white solid after purification using a silica gel column (EtOAc/hexanes 1:5 (0.5% HOAc) as eluent). ^{1}H NMR (500 MHz, $CDCl_3$): δ 11.43 (brs, 1H), 7.32 (d, J = 8.8 Hz, 2H), 7.29 (d, J = 8.8 Hz, 2H), 5.27 (s, 1H), 2.34 (s, 3H). ^{13}C NMR (100 MHz, $CDCl_3$): δ 193.5, 175.4, 134.7, 132.7, 129.5, 128.6, 50.1, 30.0. HRMS (M + Na^+) (ESI) calcd for $C_{10}H_9ClO_3SNa^+$ 266.9849, found 266.9846.

***S*-Acetyl-α-(*p*-methoxyphenyl)-α-mercaptoacetic Acid (2d).** Compound **2d** (1.75 g, 7.3 mmol, yield 73%) was obtained as a white solid after purification by silica gel column chromatography (EtOAc/hexanes 1:2 (0.5% HOAc) as eluent). ^{1}H NMR (400 MHz, $CDCl_3$): δ 9.60 (brs, 1H), 7.32 (d, J = 8.7 Hz, 2H), 6.86 (d, J = 8.7 Hz, 2H), 5.26 (s, 1H), 3.79 (s, 3H), 2.35 (s, 3H). ^{13}C NMR (100 MHz, $CDCl_3$): δ 194.1, 175.5, 159.9, 129.7, 125.9, 114.4, 55.3, 50.3, 29.9. HRMS (M + Na^+) (ESI) calcd for $C_{11}H_{12}O_4SNa^+$ 263.0354, found 263.0350.

General Synthesis of 4-(Aryl)-1,3,2-oxathiazolylium-5-olate (3a−3d). Compound **2a**, **2b**, **2c**, or **2d** (7−8 mmol) was dissolved in anhydrous MeOH (120 mL). The solution was flushed with Ar for 5 min, and then sodium methoxide was gradually added until the pH reached 9−10. After the mixture was stirred for 5 h under N_2 at room temperature, the acid resin (Amberlyst 15 ion-exchange resin) was added to ensure a pH of 2−3. The resin was then removed by filtration, and the solvent was evaporated. The residue was dissolved in dry CH_2Cl_2 (50 mL) and was allowed to cool in an ice bath. Isobutylnitrite (1.9 mL, 16 mmol) was added and stirred for 2 h while the mixture was protected from light. The reaction mixture was diluted with dry CH_2Cl_2 (200 mL), and DCC (5.00 g, 24 mmol) was added. The mixture was stirred for an additional 2 h at 0 °C, and H_2O (0.3 mL) was added to quench the reaction. The reaction mixture was passed through a Celite pad, and the filtrate was concentrated and purified by silica gel column chromatography using EtOAc/hexanes 1:10 as the eluent.

4-(*p*-Trifluoromethylphenyl)-1,3,2-oxathiazolylium-5-olate (3a). For compound **2a**, 2.27 g, 8.17 mmol was used. Compound **3a** (1.16 g, 4.70 mmol, yield 58%) was obtained as yellow needle crystals. ^{1}H NMR (500 MHz, $CDCl_3$): δ 8.11 (d, J = 8.3 Hz, 2H), 7.88 (d, J = 8.3 Hz, 2H). ^{13}C NMR (100 MHz, $CDCl_3$): δ 174.7, 132.0 (q, J = 33.0 Hz), 129.7, 126.5 (q, J = 4.0 Hz), 126.1, 123.5 (q, J = 270.0 Hz), 119.1. HRMS (M + Na^+) (ESI) calcd for $C_9H_4F_3NO_2SNa^+$ 269.9813, found 269.9813.

4-Phenyl-1,3,2-oxathiazolylium-5-olate (3b). For compound **2b**, 1.68 g, 8.0 mmol was used. Compound **3b** (916 mg, 5.02 mmol, yield 64%) was obtained as yellow needle crystals. ^{1}H NMR (400 MHz, $CDCl_3$): δ 7.89 (d, J = 7.8 Hz, 2H), 7.51−7.48 (m, 3H). ^{13}C NMR (100 MHz, $CDCl_3$): δ 174.9, 130.0, 129.2, 126.6, 126.0, 120.4. HRMS (M + Na^+) (ESI) calcd for $C_8H_5NO_2SNa^+$ 201.9939, found 201.9941.

4-(*p*-Chlorophenyl)-1,3,2-oxathiazolylium-5-olate (3c). For compound **2c**, 1.76 g, 7.2 mmol was used. Compound **3c** (1.16 g, 4.70 mmol, yield 58%) was obtained as yellow needle crystals. ^{1}H NMR (400 MHz, $CDCl_3$): δ 7.92 (d, J = 8.3 Hz, 2H), 7.59 (d, J = 8.3 Hz, 2H). ^{13}C NMR (100 MHz, $CDCl_3$) δ 175.4, 134.9, 129.7, 128.1, 126.1, 120.0, 83.7. HRMS (M + Na^+) (ESI) calcd for $C_8H_4ClNO_2SNa^+$ 235.9545, found 235.9540.

4-(*p*-Methoxyphenyl)-1,3,2-oxathiazolylium-5-olate (3d). For compound **2d**, 1.75 g, 7.3 mmol was used. Compound **3d** (823 mg, 3.94 mmol, yield 54%) was obtained as yellow needle crystals. ^{1}H NMR (250 MHz, $CDCl_3$): δ 8.87 (d, J = 8.9 Hz, 2H), 8.09 (d, J = 8.9 Hz, 2H). ^{13}C NMR (63 MHz, $CDCl_3$): δ 175.0, 160.7, 127.7, 121.1, 119.1, 114.8, 55.5. HRMS (M + Na^+) (ESI) calcd for $C_9H_7NO_3SNa^+$ 232.0044, found 232.0046.

Decomposition Studies of 3a−3d. In each study, UV−vis absorbance reading of the solvent was used to correct the actual readings from the samples. All solutions were protected from light by covering the exposed parts of the cuvette with aluminum foil, and the absorbance reading was monitored at the wavelengths of 580, 587, 592, and 602 nm for **3a**−**3d**, respectively, at 37 °C. Acidic condition: 0.8 mM solutions of compounds **3a**−**3d** were prepared in a mixture of 0.1 M phosphate buffer (882 μL, pH 5.0) and acetonitrile (98 μL). The absorbances of **3a**, **3b**, **3c**, or **3d** were immediately monitored over a period of 5, 40, 80, or 500 min, respectively. Neutral condition: 0.4 mM solution of **3b** was prepared in 0.1 M Tris-HCl buffer (882 μL, pH 7.0) and acetonitrile (98 μL) solvent system. The absorbance was monitored for 20 h. Acetonitrile: Decomposition studies of **3a**−**3d** (0.4 mM) in acetonitrile were also carried out, and absorbance readings were monitored for 2 h. Presence of room light: 1 mL of a solution of 0.4 mM **3b** in 0.1 M phosphate buffer (882 μL, pH 7.0) and acetonitrile (98 μL) was exposed to room light, and the decay of absorbance was monitored over a period of 3 h. Similar experiment was done using a 0.8 mM solution of *S*-nitrosoglutathione (GSNO) using the same solvent system. Presence of Fe^{2+}: $Fe(NH_4)_2(SO_4)_2$ (10 μM) solution was added to a solution of **3b** (0.4 mM) in PBS buffer. Likewise, $Fe(NH_4)_2(SO_4)_2$ (20 μM) solution was added to a solution of GSNO (0.8 mM) in PBS

buffer. The decay of absorbances at wavelengths 587 and 335 nm was monitored for **3b** and GSNO, respectively, over a period of 20 min.

Acid Catalysis of 3b. Various solutions at pH 5.0, 5.5, 6.0, 6.5, and 7.0 of 0.4 mM **3b** in 0.1 M phosphate buffer (882 μL) and acetonitrile (98 μL) were used. The absorbance of **3b** was immediately monitored over a period of 10 min for each solution. The rate constant for the decomposition was obtained by plotting the ln of concentration versus time for the first 5 min, and the slope was calculated using the equation $\ln[\mathbf{3b}] = -k \cdot t = -k'[H^+] \cdot t$.

EPR Spin Traps. Materials. The spin trap, 5,5-dimethyl-1-pyrroline *N*-oxide (DMPO) and *N*-benzylidene-*tert*-butylamine *N*-oxide (PBN) >99%, were obtained commercially and showed no paramagnetic impurities. Sodium *N*-methyl-D-glucamine dithiocarbamate (MGD) was synthesized using the procedure developed by Shinobu et al.[71] Phosphate-buffer saline (pH 7.0) was used with 100 μM diethylenetriaminepentaacetic acid (DTPA) as a metal chelating agent for spin trapping studies using DMPO and PBN.

Preparation of [$(MGD)_2$−Fe^{II}] Complex. Freshly prepared [$(MGD)_2$−Fe^{II}] was used in all of the NO-trapping studies by dissolving MGD (790 mg, 3 mmol) in 10 mL of distilled water. The solution was then purged with Ar gas for ∼5−10 min, and $Fe(NH_4)_2(SO_4)_2 \cdot 6H_2O$ (390 mg, 1 mmol) was added. [$(MGD)_2$−Fe^{II}] gave a clear yellowish solution, which oxidizes to a dark brown solution over time.[49]

EPR Measurements. EPR measurements were carried out at room temperature on an EMX X-band spectrometer equipped with HS resonator. General instrument settings are as follows. NO-trapping: microwave power, 20 mW; modulation amplitude, 4.00 G; receiver gain, 2.00×10^5; scan time, 42 s; time constant, 82 ms; sweep width 80 G. S-centered radical trapping: microwave power, 20 mW; modulation amplitude, 1.00 G; receiver gain, 2.00×10^5; scan time, 42 s; time constant, 164 ms; sweep width 100 G. Measurements were performed using a 50 μL glass capillary tube.

Spin Trapping of Nitric Oxide from 3a−3d. Method I. Purging with argon: Nitric oxide was generated in a 5 mL conical flask by adding 20 mM DMSO solution of **3a**−**3d** to a PBS buffer containing 100 μM DTPA. It should be noted that the pH of PBS with 50% DMSO alone is ∼10. The pH was carefully adjusted to ∼5.0 by adding 1 M H_2SO_4. The flask was covered with a rubber septa and purged with Ar using a needle syringe. The purged gas was allowed to flow through a tube connected to a separate reaction vessel containing 1 mL of 10 mM [$(MGD)_2$−Fe^{II}]. EPR spectrum was obtained for each 50 μL of [$(MGD)_2$−Fe^{II}] solution taken at various time intervals. This procedure was repeated without H_2SO_4 as the acid control. Method II. Direct mixing: In a typical experiment, the NO adduct was generated from 50 μL of PBS solution containing [$(MGD)_2$−Fe^{II}] (20 mM) and **3a**−**3d** (20 mM, note: stock solutions of **3a**−**3d** are in DMSO). The pH of the solution was carefully adjusted to ∼5 by adding 1 M H_2SO_4. The mixture was transferred to a 50 μL capillary tube and was used for EPR measurements. The formation of the low-field peak intensity was monitored over a period of 13 min. This procedure was repeated without acidification. Quantitation of the intensities was performed using the signal intensity of the first low-field peak arising from the [$(MGD)_2$−Fe^{II}−NO] adduct, which was generated from 0.6 to 6.0 mM (with an increment of 0.6 mM) of *S*-nitroso-*N*-acetylpenicillamine (SNAP) in the presence of [$(MGD)_2$−Fe^{II}].

Spin Trapping of Sulfur-Centered Radical Intermediate from Compounds 3a−3d. Spin trapping of S-centered radical intermediate was carried out using DMPO. In a typical experiment, the pH of 50 μL of PBS buffer solution containing DMPO (200 mM) and **3a**, **3b**, **3c**, or **3d** (20 mM) was adjusted to pH ∼5 by addition of 1 M H_2SO_4. The formation of the low-field EPR peak intensity was monitored over a period of 20 min using the time-sweep setting. This procedure was repeated without acidification of the solution. Peak intensities were quantified using 1−8 mM (at increment of 2 mM) solutions of 2,2,5,5-tetramethyl-3-pyrrolin-1-oxyl-3-carboxylic acid (3-CP) in PBS. Spin trapping of thiyl radical intermediate generated from **3b** was also carried out using α-phenyl-*tert*-*N*-butyl nitrone (PBN) as spin trap. The pH of PBN (200 mM) and **3b** (20 mM) PBS solution was adjusted to pH ∼5 by addition of 1 M H_2SO_4, and the formation of spin adduct was monitored by EPR. The EPR spectrum was also obtained using PBS solution of PBN (200 mM), H_2O_2 (20 mM), and ∼100 μM $FeCl_2$ for comparison.

Stability Studies. Stability of compounds **3a**−**3d** in the presence of ascorbic acid and glutathione was investigated. EPR measurements were carried out using PBS solution of 200 mM DMPO, 20 mM **3a**−**3d**, 1 mM L-ascorbic acid, or 1 mM reduced L-(−)-glutathione. Spectrophotometric analysis of the reaction mixture was carried out using a solution of 0.5 mM **3a** and 0.1 mM l-ascorbic acid. Peak decay at 581 nm was monitored. This procedure was repeated using 0.1 mM reduced glutathione.

Mass Spectral Analysis. Electrospray ionization (ESI) mass spectrometric analyses were performed immediately on the acidified and nonacidified solutions of **3a** (0.1 mM) in DMSO. Mass analyses were performed with a 3-tesla Fourier transform mass spectrometer in positive ion detection.

Cyclic Voltammetry Measurements. Cyclic voltammetry was performed using a potentiostat, and Ag/AgCl (0.01 M) as reference electrode, platinum electrode as the working electrode, and an auxiliary electrode. The concentration of **3a**−**3d** used was 0.1 mM in 1 mM tetrabutylammonium tetrafluoroborate ($TBABF_4$) in acetonitrile.

General Computational Methods. The initial conformational search was carried out using the OPLS2001 force field of the Macromodel/Maestro software package. Density functional theory[72,73] was applied in this study to determine the optimized geometry, vibrational frequencies, and single-point energy of all stationary points.[74−77] To include solvation effects into our calculations, polarizable continuum model (PCM)[78−82] calculation was performed on the single-point energies. All calculations were done using Gaussian 03[83] at the Ohio Supercomputer Center. Single-point energies were obtained at the B3LYP/6-31+G** level based on the optimized B3LYP/6-31G* geometries. Natural population analyses (NPA)[84] were also performed at the B3LYP/6-31+G** level of theory. These basis set calculations used the standard six Cartesian d functions. Stationary points for all compounds have zero imaginary vibrational frequencies as derived from a vibrational frequency analysis (B3LYP/6-31G*). A scaling factor of 0.9806 was used for the zero-point vibrational energy (ZPE) corrections with the B3LYP/6-31G* level of theory.[85] Spin contamination for all of the stationary point of the radical structures was negligible, that is, $0.75 < \langle S^2 \rangle < 0.78$.

Vascular Reactivity Study. Contraction and relaxation of isolated aortic rings were measured in an organ bath containing modified Krebs−Henseleit solution (118 mM NaCl, 24 mM Na_2HCO_3, 4.6 mM KCl, 1.2 mM NaH_2PO_4, 1.2 mM $CaCl_2$, 4.6 mM HEPES, and 18 mM glucose) aerated with 95% CO_2−5% O_2, 37 °C, and pH 6.5. Aortic

(71) Shinobu, L. A.; Jones, S. G.; Jones, M. M. *Acta Pharm. Toxicol.* **1984**, *54*, 189.
(72) Labanowski, J. W.; Andzelm, J. *Density Functional Methods in Chemistry*; Springer: New York, 1991.
(73) Parr, R. G.; Yang, W. *Density Functional Theory in Atoms and Molecules*; Oxford University Press: New York, 1989.
(74) Becke, A. D. *Phys. Rev.* **1988**, *38*, 3098.
(75) Lee, C.; Yang, W.; Parr, R. G. *Phys. Rev. B* **1988**, *37*, 785.
(76) Becke, A. D. *J. Chem. Phys.* **1993**, *98*, 1372.
(77) Hehre, W. J.; Radom, L.; Schleyer, P. V.; Pople, J. A. *Ab Initio Molecular Orbital Theory*; John Wiley & Sons: New York, 1986.
(78) Tomasi, J.; Persico, M. *Chem. Rev.* **1994**, *94*, 2027.
(79) Cossi, M.; Barone, V.; Cammi, R.; Tomasi, J. *Chem. Phys. Lett.* **1996**, *255*, 327.
(80) Barone, V.; Cossi, M.; Tomasi, J. *J. Chem. Phys.* **1997**, *107*, 3210.
(81) Barone, V.; Bencini, A.; Cossi, M.; Di Matteo, A.; Mattesini, M.; Totti, F. *J. Am. Chem. Soc.* **1998**, *120*, 7069.
(82) Tomasi, J.; Mennucci, B.; Cammi, R. *Chem. Rev.* **2005**, *105*, 2999.
(83) Frisch, M. J.; et al. *Gaussian 03*, revision B.04; Gaussian, Inc.: Pittsburgh, PA, 2003.
(84) Reed, A. E.; Curtiss, L. A.; Weinhold, F. A. *Chem. Rev.* **1988**, *88*, 899.
(85) Scott, A. P.; Radom, L. *J. Phys. Chem.* **1996**, *100*, 16502.

rings were cut into 3 mm segments and mounted on a wire myograph (Danish Myo, GA). Contraction was measured via a force transducer interfaced with Chart software for data analysis. Following a 30 min equilibration period, the rings were stretched to generate a tension of 1.0 g. The optimum resting force of the aortic rings was determined by comparing the force developed by 40 mM KCl under varying resting force. The effects of aryloxathiazolyliumolates on vascular relaxation were then determined following phenylephrine (0.5 μM)-induced contraction. The effects of 20 μM of compounds **3a**−**3d** on vascular relaxation were then measured. Results represent the mean ± SD from $n = 4$ groups.

Conclusion

In summary, a novel series of aryloxathiazolyliumolates were developed whose NO-releasing property was controlled by the pH of their environment. Para-substitution of the aryl moiety with electron-withdrawing groups showed higher NO-releasing capabilities as compared to electron-donating substituents. The decomposition pathway was supported by detection of NO and S-centered radical intermediates using EPR spin-trapping. Also, product analysis using mass spectrometry further confirmed the formation of the various types of radical intermediates.

Computational studies suggest that the most plausible pathway for aryloxathiazolyliumolates decomposition is via acid-catalyzed concerted nucleophilic addition of water and ring opening of the RSNO pentacylic ring, similar to that observed in ester hydrolysis, and is followed by homolytic cleavage of S−N bond to form NO.

These aryloxathiazolyliumolates were also found to be stable in the presence of biological reductants. Vasodilation studies on rat aortic rings revealed that vascular relaxation in the presence of aryloxathiazolyliumolates is pH dependent where a higher vasodilating effect was observed at pH 6 than at pH 7.4. This comprehensive study demonstrated the potential application of aryloxathiazolyliumolates as future pro-drugs of *S*-nitrosothiols for the controlled NO release in biological systems.

Acknowledgment. This work is supported by a grant from the NIH (GM54074). F.A.V. acknowledges NIH grant HL081248. J.L.Z. acknowledges support from NIH grants HL38324, HL63744, and HL65608. The Ohio Supercomputer Center (OSC) is acknowledged for their generous computational support of this research. We acknowledge the Center for EPR Spectroscopy and Imaging at OSU. We also wish to thank Mr. Jie Shen for helpful discussions.

Supporting Information Available: Complete ref 83. NMR, EPR, MS, and cyclic voltammetry spectra. Geometries, energies, enthalpies, and free energies for all compounds. This material is available free of charge via the Internet at http://pubs.acs.org.

JA0682226